18th Brazilian Congress of Thermal Sciences and Engineering
November 16-20, 2020 (Online)

ENC-2020-0218
CFD SIMULATION OF ISOTHERMAL UPWARD TWO-PHASE FLOW IN A VERTICAL TUBE OF ANNULAR SECTION

Flavio Eduardo Ceravolo
Marcelo da Silva Rocha
University of Sao Paulo, Institute for Nuclear and Energy Research, IPEN/SP
flavioceravolo@usp.br
msrocha@ipen.br

Delvonei Andrade
University of Sao Paulo, Institute for Nuclear and Energy Research, IPEN/SP
delvonei@ipen.br

Abstract. *This work presents a simulation of a vertical, upward, isothermal two-phase flow of air bubbles and water in an annular channel applying a Computational Fluid Dynamics (CFD) code. The simulation considers an Eulerian frame, with a two-fluid model, specific correlations for turbulence modeling, and bubble-induced turbulence effects. The work intends to assess the accuracy of the code by comparing the simulation results with experimental data obtained from the literature. The annular channel has an equivalent hydraulic diameter of 19.1 mm, where the outer pipe has an internal diameter of 38.1 mm, the inner cylinder 19.1 mm, and a total length of 1900 mm. The void fraction distribution, taken radially to the flow section, is the main parameter analyzed besides interfacial area concentration (IAC), interfacial gas velocity, and bubble diameters distribution. The numerical models applied in this work demonstrate satisfactory agreement with the experimental data but indicate the need for further improvement in the phase interaction models.*

Keywords: *Bubble column, two-phase flow, annular flow, CFD.*

1. INTRODUCTION

The study of isothermal gas-liquid flow in annular channels can provide a research basis for more complex systems such as a reboiler in a distillation column or the flow channel in a fuel rod of a BWR nuclear reactor. Several experimental studies using annular flow have been conducted in the literature to study interfacial area transport mechanisms and void fraction (or gas volume fraction) in liquid-gas flow to validate models representing such a phenomenon (Hibiki & Ishii, 2002).

This work aims to apply the CFD code ANSYS® Academic Research Fluent 19.0 (ANSYS 19.0, 2018) to the representation of an isothermal rising air-water flow in an annulus channel. For this, experimental data from (Hibiki, Situ, et al., 2003) are used for comparison with the numerical models applied.

2. MATHEMATICAL MODELING OF TWO-PHASE FLOWS

The mathematical model is based on the two-fluid model approach (Ishii & Hibiki, 2011), which is divided into a set of equations for each phase describing the conservation of mass, momentum, and energy, as well as the closure relations to address the turbulence phenomena and the interaction forces between the phases.

2.1. Mass conservation equation

The Eq. (1) represents the continuity of mass for each phase *k*, disregarding the mass transfer at the interface since this it is assumed valid for the isothermal air-water flow in the present work.

$$\frac{\partial}{\partial t}(\alpha_k \rho_k) + \nabla \cdot (\alpha_k \rho_k \mathbf{v_k}) = 0 \tag{1}$$

The term α_k represents the volume fraction of phase *k*, ρ_k its density, and $\boldsymbol{v}_k$ corresponds to the phase velocity.

2.2. Momentum conservation equation

The momentum balance of each phase is given by:

$$\frac{\partial}{\partial t}(\alpha_k \rho_k \mathbf{v_k}) + \nabla \cdot (\alpha_k \rho_k \mathbf{v_k} \mathbf{v_k}) = -\alpha_k \nabla P - \nabla \cdot (\alpha_k \boldsymbol{\tau_k}) + \alpha_k \rho_k \mathbf{g} + \mathbf{F} \quad (2)$$

where the term *P* is the pressure at which the phases are subjected, $\boldsymbol{g}$ the gravity acceleration, $\boldsymbol{F}$ stands for the external forces acting over the phases, and $\boldsymbol{\tau_k}$ is the stress tensor given by:

$$\boldsymbol{\tau_k} = -\mu_{eff,L}[(\nabla \mathbf{v_k}) + (\nabla \mathbf{v_k}^{\mathbf{T}}) - \frac{2}{3}(\nabla \mathbf{v_k})\,\mathbf{I}] \quad (3)$$

Here the term **I** is the unit tensor, and $\mu_{eff,L}$ is the effective viscosity of the liquid according to:

$$\mu_{eff,L} = \mu_L + \mu_{T,L} + \mu_{BIT,L} \quad (4)$$

The terms μ_L, $\mu_{T,L}$ and $\mu_{BIT,L}$ correspond respectively to the molecular viscosity, the viscosity resulting from turbulence, and viscosity due to the bubble-induced turbulence (BIT).

For the gas phase the effective viscosity, $\mu_{eff,G}$, is given by the following ratio:

$$\mu_{eff,G} = \mu_{eff,L} \frac{\rho_G}{\rho_L} \quad (5)$$

where ρ_G and ρ_L are the gas and liquid phase densities.

2.2.1. Modeling the Interfacial Forces

In the two-fluid model, the interfacial transfer phenomena strongly depend on the adopted constitutive relationships to describe the interaction between the phases. In this work, the momentum source term $\boldsymbol{F}$ (Eq. (2)) incorporates the effect of drag force $\boldsymbol{F}_{drag}$, lift force $\boldsymbol{F}_{lift}$, wall lubrication force $\boldsymbol{F}_{wl}$, and turbulent dispersion force $\boldsymbol{F}_{td}$. The following sections address the models applied to describe each source term.

2.2.1.1. Drag Force

A particle flowing in a liquid medium is subjected to drag and lift force. The drag force arises parallel and in the opposite direction to the flow, while the lift force, arises orthogonally to the flow. The drag momentum source depends on the relative velocity between the phases, as it is given by:

$$F_{drag} = \frac{3}{4}\frac{C_D}{d_b}\alpha_G \rho_L |\mathbf{v_G} - \mathbf{v_L}|(\mathbf{v_L} - \mathbf{v_G}) \quad (6)$$

Here the drag force coefficient C_D is calculated according to (Schiller & Naumann, 1935) model which is an acceptable method for all fluid-fluid pairs, according to (Ansys, 2013). In this model, the drag force coefficient depends on the bubble Reynolds number, as stated by:

$$C_D = \begin{cases} \frac{24}{Re_b}(1 + 0.15 Re_b^{0.687}) & Re_b \leq 1000 \\ 0.44 & Re_b > 1000 \end{cases} \quad (7)$$

The bubble Reynolds number, Re_b, is defined by:

$$\mathrm{Re_b} = \frac{\rho_L |\mathbf{v_G} - \mathbf{v_L}| d_b}{\mu_L} \tag{8}$$

2.2.1.2. Lift force

In a vertical upward flow, a bubble experiences a force pointing perpendicularly to the flow direction, mainly due to the velocity gradients in the liquid phase. Here the momentum source, related to the lift force, is modeled according to the work of (Drew & Lahey, 1993):

$$\mathrm{F_{lift}} = -C_l \rho_L \alpha_G (\mathbf{v_L} - \mathbf{v_G}) \times (\nabla \times \mathbf{v_G}) \tag{9}$$

where C_l is the lift force coefficient, ρ_L is the density of the liquid phase, α_G the volumetric fraction of the gas phase, $\boldsymbol{v_L}$ the velocity of the liquid phase and $\boldsymbol{v_G}$ the velocity of the gas phase.

In order to calculate the lift coefficient C_l, here is considered the correlation of (Tomiyama et al., 2002) which applies to ellipsoidal, spherical, and cap bubbles. For spherical bubbles the model generates a positive coefficient, forcing the bubbles to the wall, while for large and distorted bubbles, a negative coefficient is generated forcing the bubbles to the core of the channel, according to the following equation:

$$C_l = \begin{cases} \text{mín.}\left[0.288\tanh\left(0.121 Re_p\right);\ 0.00105 Eo'^3 - 0.0159 Eo'^2 - 0.0204 Eo' + 0.474\right] & Eo' \le 4 \\ 0.00105 Eo'^3 - 0.0159 Eo'^2 - 0.0204 Eo' + 0.474 & 4 < Eo' \le 10 \\ -0.27 & Eo' > 10 \end{cases} \tag{10}$$

This correlation is based on the modified Eötvös number Eo' given by:

$$\mathrm{Eo'} = \frac{g(\rho_L - \rho_G) d'^2_b}{\sigma} \tag{11}$$

where d'_b is the largest dimension of a deformed bubble, as follows:

$$\mathrm{d'_b} = d_b (1 + 0.163 Eo^{0.757})^{1/3} \tag{12}$$

The usual Eötvös number, Eo represents the relationship between the thrust forces and the surface tension forces on a bubble subject to a liquid medium, as given by the equation below:

$$\mathrm{Eo} = \frac{g(\rho_L - \rho_G) d_b^2}{\sigma} \tag{13}$$

where σ is the surface tension, g is the acceleration of gravity, and d_b the bubble diameter. For a more realistic physical representation of the void fraction near the wall, the hypothesis developed by (Shaver & Podowski, 2015) is taken into account in the lift force model. It consists of a correction in the lift coefficient next to the wall, based on a nearly spherical geometry of the bubbles. The correlation proposed by the author is presented in the following equation:

$$C_{lc} = \begin{cases} 0 & \frac{y_w}{d_b} < \frac{1}{2} \\ C_l \left[3\left(\frac{2y_w}{d_b} - 1\right)^2 - 2\left(\frac{2y_w}{d_b} - 1\right)^3\right] & \frac{1}{2} \le \frac{y_w}{d_b} \le 1 \\ C_l & \frac{y_w}{d_b} > 1 \end{cases} \tag{14}$$

where C_{lc} represents the corrected value of the lift force coefficient due to the proximity with the wall. The value of y_w is the distance from the wall and d_b the bubble diameter. It can be observed that for wall distances less than half bubble diameter the correlation dumps the lift coefficient C_l, while for regions ranging between half bubble diameter and one bubble diameter, a parabolic adjust is used, and for distances greater than one bubble diameter the actual value of C_l is applied. In the work of (Lubchenko et al., 2018), due to the high void fraction results obtained adjacent to the wall (i.e.

much smaller than the bubble diameter), the correlation of (Shaver & Podowski, 2015) was successfully employed in addition to a specific model for turbulence dispersion force. A similar approach was considered by (Feng & Bolotnov, 2017) to simulate the wall forces due to the drainage around the bubbles close to the walls. Recently, the (Shaver & Podowski, 2015) correlation was also employed by (Colombo & Fairweather, 2019), (Marfaing et al., 2018), and (Sugrue et al., 2017), providing satisfactory accuracy for void fraction and gas velocity profiles.

2.2.1.3. Wall lubrication force

When a bubble moves in an infinite liquid medium the flow of liquid around the bubble is approximately symmetrical, however, when a wall is close to the bubble, the flow of liquid between the bubble and the wall creates an asymmetry in the flow around the bubble, and a hydrodynamic force pushes the bubble away from the wall. This concept is expressed by the following equation:

$$\mathbf{F}_{\mathrm{wl}} = \mathrm{C}_{\mathrm{wl}}\rho_{\mathrm{L}}\alpha_{\mathrm{G}}\left|(\mathbf{v}_{\mathrm{L}} - \mathbf{v}_{\mathrm{G}})_{||}\right|^{2} \times \mathbf{n}_{\mathrm{w}} \tag{15}$$

where C_{wl} is the wall lubrication coefficient, ρ_L the liquid phase density, α_G the gas phase volumetric fraction, $(\boldsymbol{v}_L - \boldsymbol{v}_G)_{||}$ stands for the phase relative velocity tangential to the wall, and $\boldsymbol{n}_w$ is the normal vector pointing away from the wall.

The correlation adopted for calculating the wall lubrication coefficient, C_{wl} is also derived from the work of (Antal et al., 1991) given by:

$$\mathrm{C}_{\mathrm{wl}} = \max\left(0, \frac{\mathrm{C}_{\mathrm{w1}}}{\mathrm{d}_{\mathrm{b}}} + \frac{\mathrm{C}_{\mathrm{w2}}}{\mathrm{y}_{\mathrm{w}}}\right) \tag{16}$$

where the values of the coefficients C_{w1} and C_{w2} are respectively -0.01 and 0.05 and the values of d_b and y_w correspond to the bubble diameter and the nearest distance from the wall.

2.2.1.4. Turbulent dispersion force

Turbulence in a two-phase flow creates erratic or fluctuating behavior in the relative velocity between the phases. Physically, the meaning of the turbulent dispersion is a result of the fluctuating of the component of the forces acting on the bubbles. In the simplest case, the turbulent dispersion force at one point is the average of the fluctuating component of the drag force components whose trajectories are inserted at this point (Lopez de Bertodano et al., 2006). In a liquid-gas flow in a vertical bubble column, this force acts on the dispersion of the bubbles in the direction perpendicular to the flow, "flattening" the phase distribution profiles.

The model applied in this work to describe the turbulence dispersion force is given by (Lopez de Bertodano, 1991):

$$\mathbf{F}_{\mathrm{td}} = \mathrm{C}_{\mathrm{TD}}\ \rho_{\mathrm{L}}\ \mathrm{k}_{\mathrm{L}}\nabla\alpha_{\mathrm{G}} \tag{17}$$

where ρ_L is the liquid density, k_L is turbulent kinetic energy, $\nabla\alpha_G$ is the gas volume fraction gradient and C_{TD} is an empirical constant whose default value is 1.0, however, according to (Lahey & Drew, 2001), this parameter has been adjusted between 0.1 and 1.0. Here, the turbulent dispersion constant, C_{TD} was adjusted to the value 0.2.

2.2.2. Turbulence models

In this work, the turbulence production and dissipation in the liquid phase is modeled using an adaptation for the two-phase flow of the $k-\varepsilon$ and $k-\omega$ models, as given by (Ansys, 2013). These models take into account the transport of the liquid phase turbulence kinetic energy k_L, and the turbulence energy dissipation rate ε_L (or turbulent frequency ω_L), both weighted with liquid phase volume fraction α_L. For the description of turbulence model, $k-\varepsilon$ is used as the reference case, as follows:

$$\frac{\partial}{\partial t}(\alpha_L \rho_L k_L) + \nabla \cdot (\alpha_L \rho_L \mathbf{v}_L k_L) = \nabla \cdot \left(\alpha_L \left(\mu_L + \frac{\mu_{T,L}}{\sigma_k}\right) \nabla k_L\right) + \alpha_L G_{k,L} - \alpha_L \rho_L \varepsilon_L + \alpha_L \rho_L S_{k,L} \quad (18)$$

$$\frac{\partial}{\partial t}(\alpha_L \rho_L \varepsilon_L) + \nabla \cdot (\alpha_L \rho_L \mathbf{v}_L \varepsilon_L) = \nabla \cdot \left(\alpha_L \left(\mu_L + \frac{\mu_{T,L}}{\sigma_\varepsilon}\right) \nabla \varepsilon_L\right) + \alpha_L \frac{\varepsilon_L}{k_L}\left(C_{1\varepsilon} G_{k,L} - C_{2\varepsilon} \rho_L \varepsilon_L\right) + \alpha_L \rho_L S_{\varepsilon,L} \quad (19)$$

In the above equations, for the liquid phase, α_L is the volumetric fraction, ρ_L the density, μ_L the molecular viscosity, $G_{k,L}$ the production of turbulence kinetic energy, and $\mu_{T,L}$ the turbulent viscosity is given by:

$$\mu_{T,L} = \rho_L C_\mu \frac{{k_L}^2}{\varepsilon_L} \quad (20)$$

The following constants are considered $C_\mu = 0.09$, $C_{1\varepsilon} = 1.44$, $C_{2\varepsilon} = 1.90$, $\sigma_k = 1.00$, and $\sigma_\varepsilon = 1.20$. The parameters $S_{k,L}$ and $S_{\varepsilon,L}$ refer to the source terms due to bubble-induced turbulence (BIT), which in the present work are replaced by the (Sato & Sekoguchi, 1975) model, as follows:

$$\mu_{BIT,L} = C_{\mu,G} \rho_L \alpha_G d_b |\mathbf{v}_G - \mathbf{v}_L| \quad (21)$$

This model simply incorporates the BIT effect, by an additional viscosity term based on the relative velocity between the phases. This way, both effects of $\mu_{T,L}$, and $\mu_{BIT,L}$ comprise the effective viscosity of the liquid phase, $\mu_{eff,L}$, as previously presented in Eq. (4). The recommended value for $C_{\mu,G}$ is 0.6 according to (Sato & Sekoguchi, 1975). This BIT approach has been widely applied in two-phase flow works, some of which being (Sharma et al., 2019), (Lopez de Bertodano et al., 1994), (Krepper et al., 2007), and (Prabhudharwadkar et al., 2012).

2.2.3. Interfacial area concentration model

In the multiphase phenomena, the transfer of mass, momentum, and energy are closely related to the interfacial area concentration (IAC) available in the medium. Therefore, the following equation is employed to take into account this property in the present study.

$$\frac{\partial}{\partial t}(\rho_G X) + \nabla \cdot (\rho_G \mathbf{u}_G X) = \frac{1}{3}\frac{D\rho_G}{Dt} X + \frac{2}{3}\frac{\dot{m}_G}{\alpha_G} X + \rho_G (S_{RC} + S_{TI}) \quad (22)$$

Here, X represents the IAC, ρ_G is the gas density, and α_G the gas volume fraction. The first two terms on the right hand of the Eq. (22) stand for the expansion due to the compressibility and mass transfer respectively. The parameters S_{RC} and S_{TI} correspond to the source terms of random collision coalescence and turbulent-induced breakage, respectively. These parameters are obtained by the (Hibiki & Ishii, 2000) model.

From the determination of IAC, it is possible to obtain the bubble mean diameter in a given region of the flow through the Sauter mean diameter, as follows:

$$d_b = \frac{6\alpha_G}{X} \quad (23)$$

The Sauter mean diameter is defined as the diameter of a sphere having the same area-to-volume ratio as the particle of interest.

3. MODEL IMPLEMENTATION

The geometry applied in the CFD model is one eight of an annulus channel with a hydraulic diameter (D_h) of 19.1 mm, where the internal diameter of the outer pipe is 38.1 mm, the inner cylinder diameter is 19.1 mm, and the channel length is 1900 mm (Figure 1a and b). A mesh sensitivity study was carried based on the methodology of (Stern et al., 2001). From this study, a discretization mesh with 161,898 elements was generated with 33 divisions in the radial, 11 divisions in angular, and 446 divisions in the axial direction, as shown in Figure 1c.

The simulation results are compared with experimental data from (Hibiki, Situ, et al., 2003) where the boundary conditions at the inlet consist of an air-water mixture at 20 °C and atmospheric pressure; void fraction (or gas volume fraction), α_G = 0.15; liquid velocity, v_L = 1.212 m s^{-1}; gas velocity v_G = 1.340 m s^{-1}; and IAC X = 290 m^{-1}. These flowing conditions are classified as a bubbly flow regimen according to (Kelessidis & Dukler, 1989) two-phase flow map for concentric annulus.

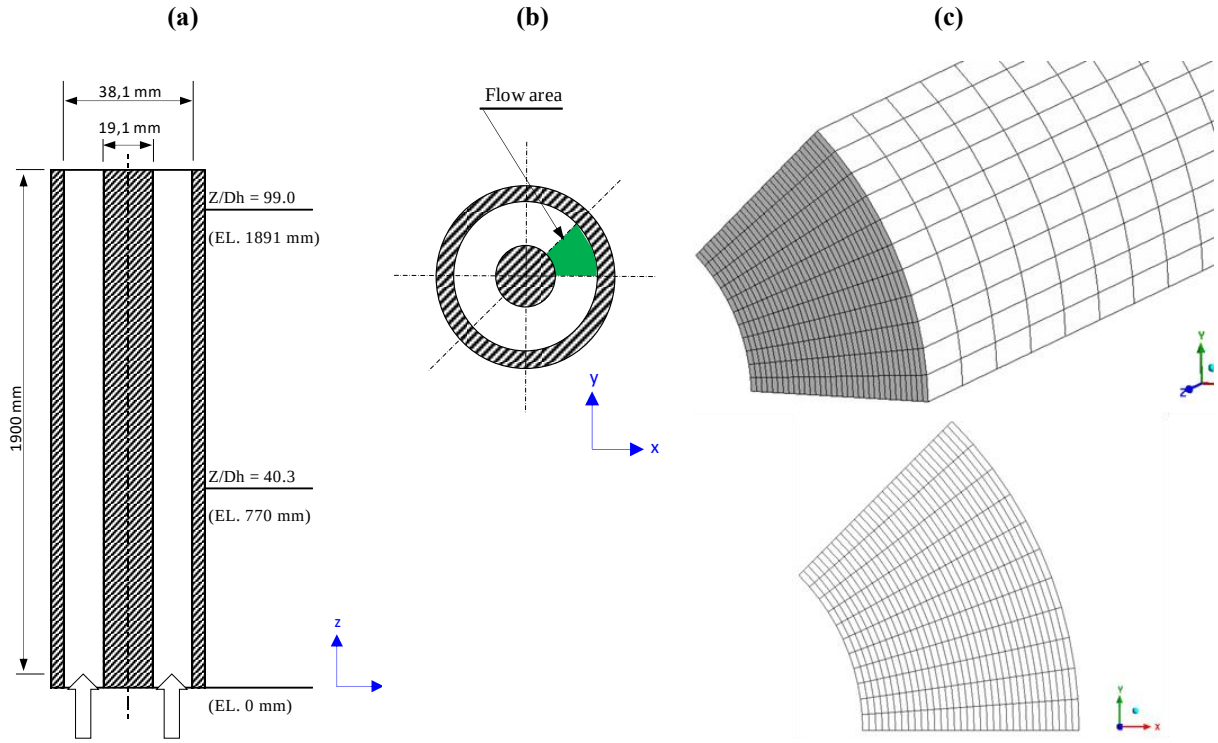

Figure 1: Schematic drawing of the annular channel (a) axial section, (b) cross-section, and (c) discretization mesh - perspective and bottom view (not to scale).

Besides that, the boundary conditions are characterized as: (i) at inlet flat profiles for all parameters; (ii) on the walls the non-slip condition for the liquid phase and free slip condition for the gas phase; and (iii) in the outlet constant pressure. The CFD simulation is conducted in transient regimen, with a time step of 0.0003 s, and it is stopped after the complete stabilization of the flow parameters in the computational domain.

The radial profiles are obtained at two axial positions from inlet z/D_h = 40.3 and 99.0, as shown in Figure 1a, which are the same elevations where the experimental data of (Hibiki, Situ, et al., 2003) were collected.

4. RESULTS AND DISCUSSIONS

Figure 2 presents the typical CFD results of void fraction in the annular channel, where it can be observed the continuous migration of the gas phase from the flat profile, at the inlet, for the walls as the lift force develops along the channel. In the same way, the Figure 3 presents the void fraction radial profiles at the two elevations of the annular channel. Due to the wall lubrication force, acting in opposition to the lift force, the void fraction results exhibit a moderate wall-peak behavior close to the inner and outer walls.

At the first measurement position (Figure 3a), the model overpredicts the void fraction in the core of the channel and the profiles close to the walls have not shown the same reduction as exhibited by the experimental data. In this case, the flat profiles assumed at inlet seems to be affecting the results as the lift and wall lubrication forces develop along the channel.

In the second measurement position (Figure 3b), the void fraction profiles are better developed as they approach the experimental data at the core of the channel. However, close to the walls the profiles do not exhibit the same reduction as observed in the experimental data. As reported by (Lubchenko et al., 2018), it can be attributed to the effect of the turbulent dispersion force which tends to flatten the void fraction profiles close to the wall, due to fluctuations in the relative velocity between the phases, leading to fluctuations in the drag forces.

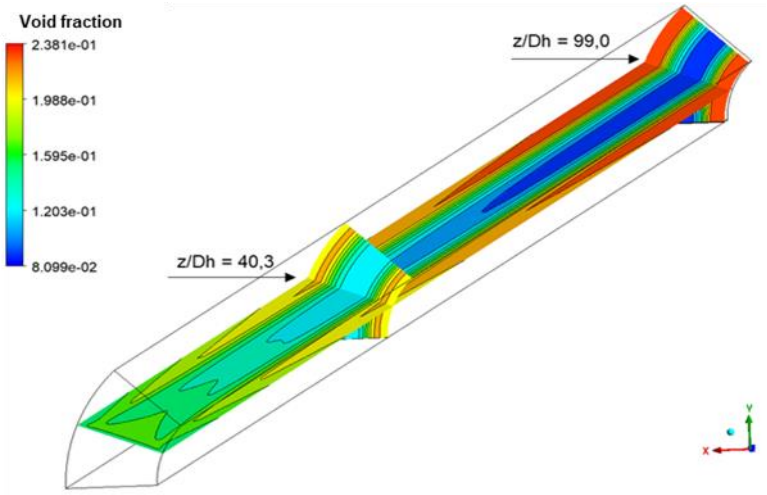

Figure 2: Void fraction results along the annular channel (not to scale).

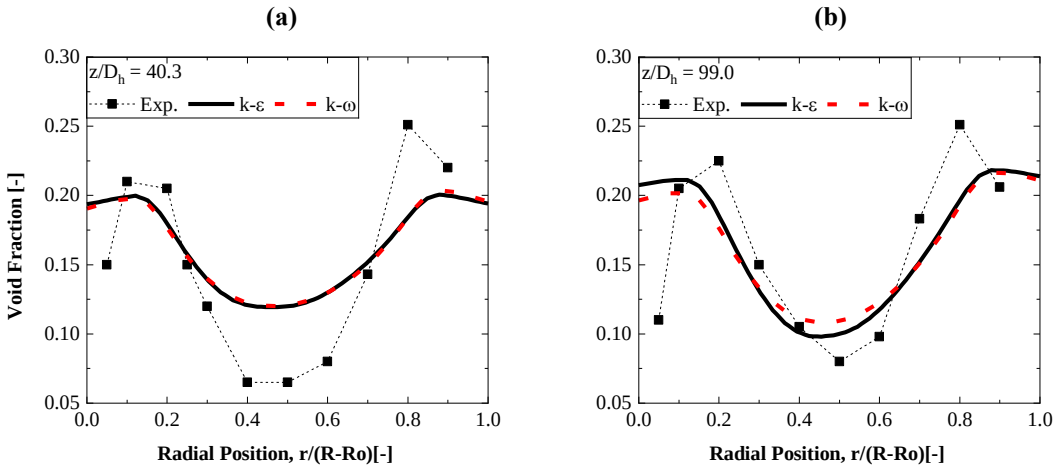

Figure 3: Void fraction profiles at the elevations (a) z/D_h=40.3 and (b) 99.0 from the inlet.

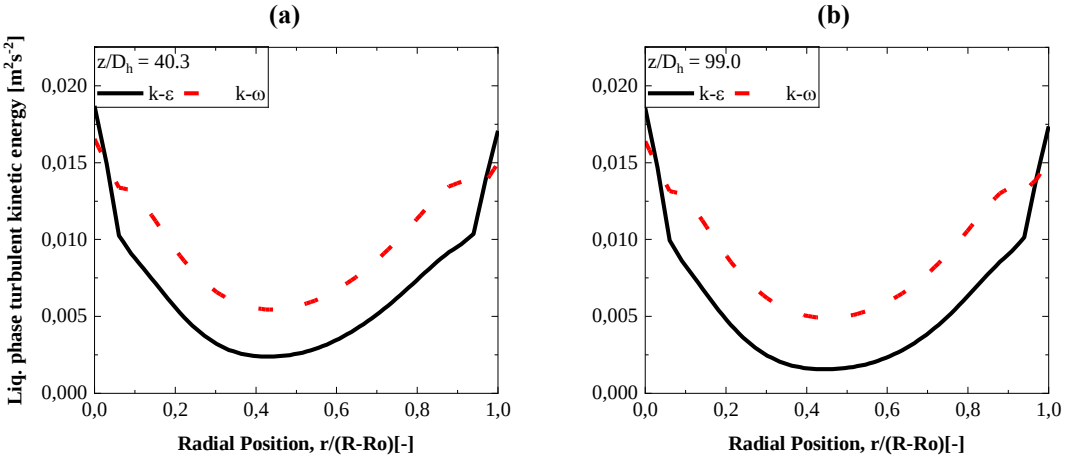

Figure 4: Liquid phase turbulent kinetic energy at the elevations (a) z/D_h = 40.3 and (b) 99.0 from the inlet.

Regarding the influence of the turbulence models, both produce similar effects on the void fraction profiles, the main differences between $k-\varepsilon$ and $k-\omega$ are observed in the second measurement position (Figure 3b), where the void fraction on the wall is slightly lower for the $k-\omega$ model, and in the core of the channel is slightly higher than for the

$k-\varepsilon$ model. It should be noted that the $k-\omega$ model produces stronger k_L profiles than $k-\varepsilon$ model, as shown Figure 4, which results in higher turbulent dispersion force, flattening the void fraction profiles, as previously noted.

In the IAC profiles it can be verified, in Figure 5, a very similar trend as the void fraction profiles (Figure 3) revealing that these parameters follow a closely constant relationship between each other. Suggesting a low interaction between the phases, which is expected in bubbly flow with low void fraction.

In Figure 6, the simulation results present a quite constant bubble size profiles that can be attributed to the low intensity of the coalescence and break-up phenomena in the flowing conditions adopted. Only in the 2nd axial position, a slight coalescence is observed close to the walls (Figure 6b), resulting in higher bubble diameters than in the core. This can be attributed to the higher turbulence dissipation produced in the 2nd measurement position than in the 1st position since the IAC coalescence and break-up source term models of (Hibiki & Ishii, 2000) are strongly affected by the turbulence dissipation parameter.

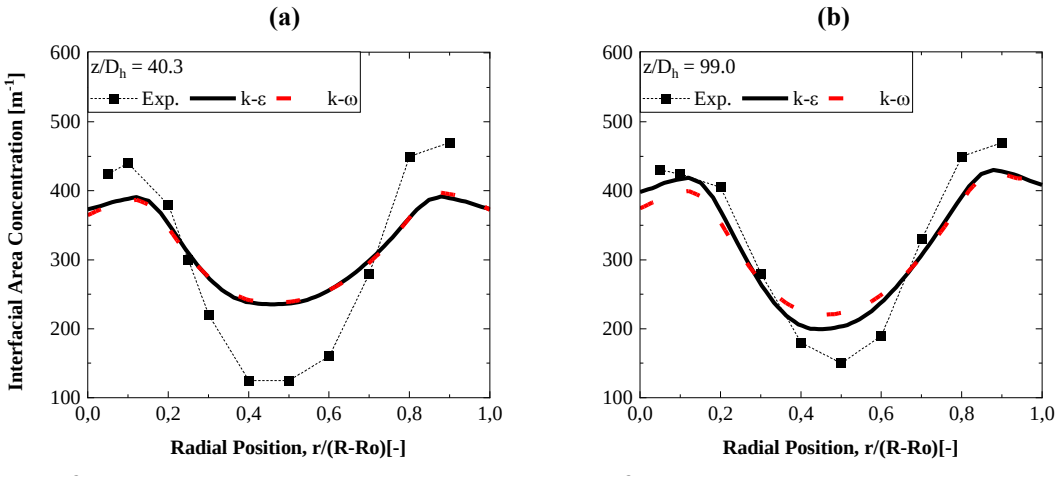

Figure 5: Interfacial area concentration at elevations (a) z/D_h = 40.3 and (b) 99.0 from the inlet.

In an opposite trend, the experimental data in Figure 6 present a reduction in the bubble diameters close to the walls, which could be interpreted as a divergence between the simulation results and the experimental data, however, according to the author of the experimental data (Hibiki, Mi, et al., 2003), the reduction in bubble sizes in these regions is because only a fraction of bubble diameter can pass close to the wall (due to the bubble curvature), in these case, the double-sensor conductivity probe, employed by the author, can measure only a fraction bubble diameter in this region. This apparent bubble reduction close to the walls has also influence in the experimental data of IAC (Figure 5), resulting in higher IAC values close to the walls.

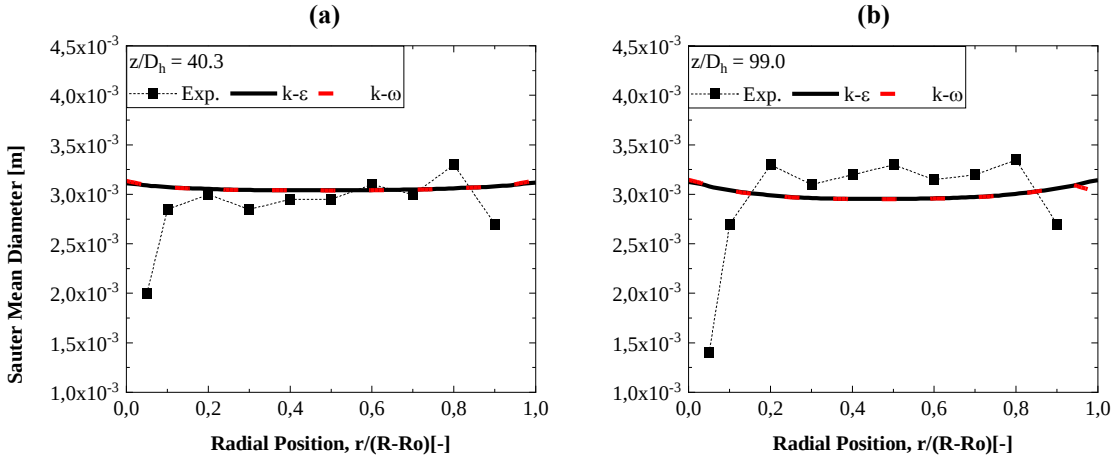

Figure 6: Bubble Sauter mean diameter at the elevations (a) z/D_h =40.3 and (b) 99.0 from the inlet.

The interfacial velocity (or gas phase velocity) profiles, in Figure 7, have shown close proximity to the experimental data, however, at the center of the channel the experimental data present a peak velocity, while the simulation results present a flatter profile. It can be attributed again to the bubble-induced turbulence since, according to (Hibiki, Situ, et al., 2003) the interfacial velocity is affected by the shear-induced turbulence, and by bubble-induced turbulence over the liquid phase.

Near to the inner and outer walls, the gas phase velocity provided good proximity to the experimental data trend, showing that the assumed boundary conditions of non-adherence to the wall, for the gas phase, provides a physically appropriate result.

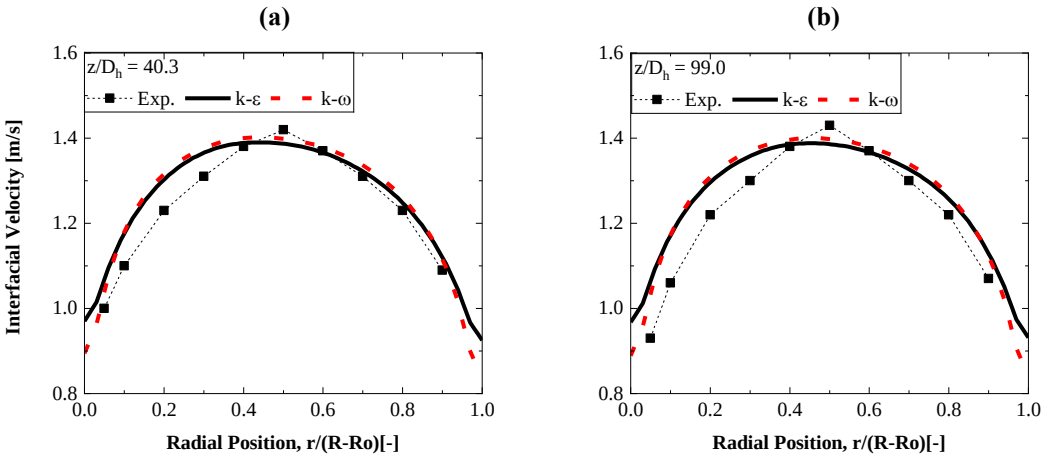

Figure 7: Interfacial velocity profiles at the elevations (a) z/D_h = 40.3 and (b) 99.0 from the inlet.

Besides that, no significant difference was observed between the turbulence models in the interfacial velocity. However, the $k-\varepsilon$ model has produced a slightly flatter velocity profile close to the wall than $k-\omega$, for both measurement points. It can be related to the higher kinetic energy turbulence produced by the $k-\varepsilon$ on the walls, as shown in Figure 4.

5. CONCLUSIONS

A numerical simulation of an upward, air-water flow in bubbly regimen, an annular channel, have been performed applying Computational Fluid Dynamics code (CFD). The numerical models used in this work demonstrated satisfactory performance in the representation of the experimental data of the literature, revealing the potential of the numerical model, however further improvements in the phase interaction models are necessary.

The void fraction profiles have exhibited a moderated wall-peak behavior in the proximity of the inner and outer walls of the annular channel, in opposition to the experimental data, which presents a strong reduction in the void fraction close to the walls. The influence of the turbulent dispersion force model seems to be over predicting the fluctuation in the liquid velocity and flattening the void fraction profiles in comparison to the experimental data. Besides, the void fraction profile seems to be strongly developing along the channel which may be due to the flat boundary conditions at the inlet.

The bubble diameter distribution profiles are fairly constant indicating that the bubble coalescence and fragmentation mechanisms are weakly affecting the IAC equation, at the flowing conditions. The bubble diameter profiles are close to the experimental data behavior except in the proximity of the walls, where the experimental data is not measuring the whole bubble diameter.

The interfacial velocity profiles have shown close proximity to the experimental, however, the flatter profile than the experimental data indicates a strong influence of the turbulence dispersion force in the model.

6. REFERENCES

Ansys, 2013. *ANSYS Fluent Theory Guide* Release 15. ANSYS, ed., Canonsburg, PA: ANSYS. Available at: http://www.ansys.com.

ANSYS 19.0, 2018. ANSYS® Academic Research Fluent.

Antal, S.P., JR, R.T.L. & Flaherty, J.E., 1991. Analysis of Phase Distribution in Fully Developed Laminar Bubbly Two-Phase Flow. *International journal of multiphase flow*, 17(No.5), pp.635–652.

Colombo, M. & Fairweather, M., 2019. Influence of multiphase turbulence modelling on interfacial momentum transfer in two-fluid Eulerian-Eulerian CFD models of bubbly flows. *Chemical Engineering Science*, 195, pp.968–984. Available at: https://doi.org/10.1016/j.ces.2018.10.043.

Drew, D.A. & Lahey, R.T., 1993. *Particulate Two-Phase Flow*, Boston, MA: Butterworth-Heinemann (January 18, 1993).

Feng, J. & Bolotnov, I.A., 2017. Interfacial force study on a single bubble in laminar and turbulent flows. *Nuclear Engineering and Design*, 313, pp.345–360. Available at: http://dx.doi.org/10.1016/j.nucengdes.2016.12.034.

Hibiki, T., Mi, Y., et al., 2003. Interfacial area transport of vertical upward bubbly two-phase flow in an annulus. *International Journal of Heat and Mass Transfer*, 46(25), pp.4949–4962. Available at: http://linkinghub.elsevier.com/retrieve/pii/S0017931003003181.

Hibiki, T., Situ, R., et al., 2003. Local flow measurements of vertical upward bubbly flow in an annulus. *International Journal of Heat and Mass Transfer*, 46(8), pp.1479–1496.

Hibiki, T. & Ishii, M., 2002. Development of one-group interfacial area transport equation in bubbly flow systems. *International Journal of Heat and Mass Transfer*, 45(11), pp.2351–2372.

Ishii, M. & Hibiki, T., 2011. *Thermo-Fluid Dynamics of Two-Phase Flow* Intergovernmental Panel on Climate Change, ed., New York, NY: Springer New York. Available at: http://ebooks.cambridge.org/ref/id/CBO9781107415324A009.

Kelessidis, V.C. & Dukler, A.E., 1989. Modeling flow pattern transitions for upward gas-liquid flow in vertical concentric and eccentric annuli. *International Journal of Multiphase Flow*, 15(2), pp.173–191.

Krepper, E. et al., 2007. Experimental and numerical studies of void fraction distribution in rectangular bubble columns. *Nuclear Engineering and Design*, 237(4), pp.399–408.

Lahey, R.T. & Drew, D.A., 2001. The analysis of two-phase flow and heat transfer using a multidimensional, four field, two-fluid model. *Nuclear Engineering and Design*, 204(1–3), pp.29–44.

Lopez de Bertodano, M. et al., 2006. Phase Distribution in the Cap Bubble Regime in a Duct. *Journal of Fluids Engineering*, 128(4), p.811. Available at: http://fluidsengineering.asmedigitalcollection.asme.org/article.aspx?articleid=1430377.

Lopez de Bertodano, M., 1991. *Turbulent Bubbly Flow in a Triangular Duct*. Rensselaer Polytechnic Institute, Troy, New York.

Lopez de Bertodano, M., Lahey, R.T. & Jones, O.C., 1994. Development of a k-ε Model for Bubbly Two-Phase Flow. *Journal of Fluids Engineering*, 116(1), p.128.

Lubchenko, N. et al., 2018. A more fundamental wall lubrication force from turbulent dispersion regularization for multiphase CFD applications. *International Journal of Multiphase Flow*, 98, pp.36–44. Available at: http://linkinghub.elsevier.com/retrieve/pii/S0301932217303713.

Marfaing, O. et al., 2018. Comparison and uncertainty quantification of two-fluid models for bubbly flows with NEPTUNE_CFD and STAR-CCM+. *Nuclear Engineering and Design*, 337(December 2017), pp.1–16.

Prabhudharwadkar, D. et al., 2012. Two-Fluid CFD Simulations of Cap Bubble Flow Using the Two-Group Interfacial Area Transport Equations. *The Journal of Computational Multiphase Flows*, 4(4), pp.363–374.

Sato, Y. & Sekoguchi, K., 1975. Liquid velocity distribution in two-phase bubble flow. *International Journal of Multiphase Flow*, 2(1), pp.79–95.

Schiller, L. & Naumann, Z., 1935. A drag coefficient correlation. *Z.Ver.Deutsch.Ing*, 77(13–14), pp.318–320.

Sharma, S.L. et al., 2019. Beyond bubbly two-phase flow investigation using a CFD three-field two-fluid model. *International Journal of Multiphase Flow*, 113, pp.1–15. Available at: https://doi.org/10.1016/j.ijmultiphaseflow.2018.12.010.

Shaver, D.R. & Podowski, M.Z., 2015. Modeling of Interfacial Forces for Bubbly Flows in Subcooled Boiling Conditions. *Transactions of the American Nuclear Society*, 113(10), pp.1368–1371.

Stern, F. et al., 2001. Comprehensive Approach to Verification and Validation of CFD Simulations—Part 1: Methodology and Procedures. *Journal of Fluids Engineering*, 123(4), p.793. Available at: http://fluidsengineering.asmedigitalcollection.asme.org/article.aspx?articleid=1484323.

Sugrue, R. et al., 2017. Assessment of a simplified set of momentum closure relations for low volume fraction regimes in STAR-CCM+ and OpenFOAM. *Annals of Nuclear Energy*, 110, pp.79–87. Available at: http://dx.doi.org/10.1016/j.anucene.2017.05.059.

Tomiyama, A. et al., 2002. Transverse migration of single bubble in simple shear flows. *Chemical Engineering Science*, 57, pp.1849–1858.

7. RESPONSIBILITY NOTICE

The authors are the only responsible for the printed material included in this paper.